Tellus (1998), 50B, 478–490
Printed in UK – all rights reserved

TELLUS
ISSN 0280–6509

The effect of cloud-processing of aerosol particles on clouds and radiation

By NIKOS HATZIANASTASSIOU‡, WOLFRAM WOBROCK and ANDREA I. FLOSSMANN*,
Laboratoire de Météorologie Physique, Université Blaise Pascal–CNRS–OPGC, 24, avenue des Landais, F-63177 Aubière Cedex, France

(Manuscript received 16 March 1998; in final form 17 June 1998)

ABSTRACT

A detailed spectral microphysics and scavenging model coupled to a dynamic framework describing a medium-sized convective cloud has been used to simulate the evolution of different clouds forming precipitation sized drops in a marine air mass. The resulting drop spectra entered a radiation code to yield the up- and downdwelling radiative fluxes, the cloud optical depth and the cloud albedo. If we start from the scenario that in a perturbed marine environment the number of small aerosol particles has doubled, this can increase the albedo of a cloud forming in this air mass of about 5% with respect to clouds forming in unperturbed conditions. This capacity to increase the cloud albedo, however, is not persistent. The cloud itself changes the particle spectrum. The smallest aerosol particles are reduced by impaction scavenging. The particles between 0.01 μm and 0.1 μm are depleted due to the fact that they serve as CCN and grow through in-cloud processes. Here, our studies have shown, however, that growth due to absorption and oxidation of gases (e.g., SO_2) plays a minor rôle and that collision and coalescence of drops is the dominant growth mechanism in a region with low gas concentrations like the remote oceans. As a result, an aerosol particle spectrum which has gained small particles due to an enhanced production of new particles seems to relax back to a spectrum similar to the previous undisturbed after cycling through some repeated cloud events.

1. Introduction

A large part of the earth's oceans is covered by shallow boundary layer clouds such as stratus or stratocumulus. They reflect parts of the incident short-wave solar radiation. At the same time they absorb and emit again long-wave terrestrial radiation. Thus, they represent an important aspect for the earth's climate. Currently, an anthropogenic change of their climate forcing is being discussed. For the marine boundary layer clouds it has been suggested that an enhanced dimethyl sulphide production by the ocean might lead to an increase in concentration of small aerosol particles, increasing the number of small cloud droplets formed, and, thus, increasing cloud albedo (Charlson et al., 1987). This enhanced cloud albedo might help to counteract the anticipated global warming due to greenhouse gases (IPCC, 1995). An effect of anthropogenically altered aerosol particle spectra on cloud albedo has been documented already for the case of shiptracks, e.g., by Ackerman et al. (1995).

However, an increase in number of small particles will also initiate a number of other processes, among those, e.g., coagulation of aerosol particles. But also clouds can be anticipated to affect the atmospheric aerosol particle spectrum. The larger particles will serve as cloud condensation nuclei

* Corresponding author.
‡ Current affiliation: Foundation for Research and Technology-Hellas; Heraklion, 71110 Crete, Greece.

(CCN) and the very small particles will be captured by drops due to brownian motion. Thus, even though the increased number of particles might alter clouds and their albedo, the clouds in turn will change the particle spectrum. Such a modification has been observed already for non-precipitating boundary layer clouds, e.g., by Hoppel et al. (1990) and Hoppel and Frick (1990). They could attribute a minimum in the particle spectrum in the range between 0.01 μm and 0.1 μm to the cycling of marine boundary layer air through shallow non-precipitating clouds.

The goal of this work is to study the interaction of marine clouds and the input and output aerosol particle spectrum on cloud albedo. Even though this interaction is proposed by Charlson et al. (1987) for marine stratiform clouds, the process should be active in all types of clouds. Thus, we have chosen as a first step to study the phenomenon for a shallow precipitating cumulus described by a simple parcel model dynamics and have coupled to this our spectral scavenging and microphysics model. The resulting drop size distributions have been used as input for the two-stream calculations in the radiation model of Zdunkowski et al. (1982) to estimate cloud albedo and optical thickness. Then, the cloud was evaporated and the residue aerosol particle spectrum was used as the input spectrum for a new cloud cycle. The modified microphysical and radiative properties of the cloud were studied.

The approach of coupling a simple parcel model with a spectral microphysics and radiation model has been tested already with data from the North Atlantic Regional Experiment (NARE) (Hatzianastassiou et al., 1997). In the present paper this approach was further compared with results from a more sophisticated dynamical framework, i.e., with the results of a 2-D model.

2. Model description

The model results presented here make use of three different modules. The first one is a dynamic module which is either a parcel model (0-D) or a 2-D model. Interactive with the dynamic framework the microphysical module is iterated. A radiative module then calculates ≪off-line≫ the radiative properties of the cloud. We will first present the modules for microphysics and radiation common to both approaches and then their coupling into the different dynamic frameworks.

2.1. *The microphysics module*

The basic framework employed in the present study is the module DESCAM, i.e., the *de*tailed *sca*venging and *m*icrophysical model as discussed in Flossmann et al. (1985, 1987). There, the aerosol particles are treated in a spectral form. Apart from dynamical processes, the number of particles of a certain size changes due to activation to drops, due to size changes resulting from humidity changes, and due to impaction scavenging by drops. The nucleated drops then grow by condensation or evaporate, collide and coalesce, and eventually break up. During their lifetime they further scavenge particles and the scavenged pollutant mass is redistributed through the microphysical processes. The extension of this microphysical and scavenging model to the scavenging of two different types of aerosol particles (e.g., $(NH_4)_2SO_4$ and NaCl for marine air masses) is described in Flossmann (1991) and the inclusion of effects of gaseous H_2O_2 and O_3 on the uptake and oxidation of SO_2 was presented in Flossmann (1994). Currently, the model contains prognostic equations for 11 distribution functions as summarised in Table 1. For further details on the terms changing the density distribution functions see Flossmann et al. (1985) and Flossmann (1994).

2.2. *The radiation module*

The radiation model used is described by Zdunkowski et al. (1982) and has already been applied in connection with DESCAM in Hatzianastassiou et al. (1997). It treats the multiple scattering with a practical improved flux method (Zdunkowski et al., 1980) for the solar spectrum and the atmospheric window region. For the remaining infrared spectrum an extended emissitivity method is used, taking into account all overlapping effects and grey clouds. The accuracy of this method is discussed by Zdunkowski and Breslin (1979). The model incorporates the effects of atmospheric water vapour, carbon dioxide, ozone, pollution gases such as NO_2, as well as dry air and aerosol particles. The spectral integration is made in six spectral intervals covering the short wave (SW) and infrared (IR) regions. The optical properties of atmospheric gases permit the

Table 1. *11 density distribution functions as used in the DESCAM model with m being the drop mass and m_{AP} being the aerosol particle mass; the drop and aerosol particle categories are logarithmically equally spaced with a mass doubling every second category*

Density distribution function		No. classes, minimum and maximum radius
$f_d(m)$	drop number density distribution function	69, 1 μm–2580 μm
$g_{APd,(NH_4)_2SO_4}(m)$	mass density distribution function for $(NH_4)_2SO_4$ particles in the drops	69, 1 μm–2580 μm
$g_{APd,NaCl}(m)$	mass density distribution function for NaCl particles in the drops	69, 1 μm–2580 μm
$g_{Gd,S(4)}(m)$	mass density distribution function for the sulfur species S(4) in the drops	69, 1 μm–2580 μm
$g_{Gd,S(6)}(m)$	mass density distribution function for the sulfur species S(6) in the drops	69, 1 μm–2580 μm
$g_{Gd,H_2O_2}(m)$	mass density distribution function for H_2O_2 gas in the drops	69, 1 μm–2580 μm
$g_{Gd,O3}(m)$	mass density distribution function for O_3 gas in the drops	69, 1 μm–2580 μm
$f_{APa,(NH_4)_2SO_4}(m_{AP})$	aerosol particle number density distribution function for $(NH_4)_2SO_4$ particles in the air	81, 10^{-3} μm–10 μm
$f_{APa,NaCl}(m_{AP})$	aerosol particle number density distribution function for NaCl particles in the air	81, 10^{-3} μm–10 μm
$g_{APa,(NH_4)_2SO_4}(m_{AP})$	the mass density distribution function for $(NH_4)_2SO_4$ particles in the air	81, 10^{-3} μm–10 μm
$g_{APa,NaCl}(m_{AP})$	the mass density distribution function for NaCl particles in the air	81, 10^{-3} μm–10 μm

splitting of the IR emission spectrum into two major spectral intervals. In the window region (8.75–12.25 μm) the gaseous absorption is relatively weak so that scattering effects by particles are considered. In the remaining IR spectral interval (3.7–8.75 and 12.25–100 μm), scattering effects are neglected owing to the dominant gas and droplet absorption. The complexity of the solar absorption of atmospheric gases as well as the significant wavelength dependence of droplet absorption, require the subdivision of the SW spectrum into four intervals: (0.28–1.0 μm), (1.0–1.53 μm), (1.53–2.2 μm) and (2.2–6.0 μm). The model requires also the extinction and absorption coefficients as well as the asymmetry factor of the phase function for the water droplet and the aerosol particle spectra. These quantities are derived by Mie calculations for the droplet and aerosol particle spectra of the DESCAM output. The composition of the cloud particles is taken into account through the calculation of the refractive indices (real and imaginary) for the individual components of each cloud constituent (see Hatzianastassiou et al., 1997).

2.3. *The microphysical and radiative module in the air parcel framework*

The dynamics of the rising and entraining air parcel and its coupling to the DESCAM module has been described, e.g., in Flossman et al. (1985). The combination yields the dynamic, thermodynamic and microphysics every 2 s which represents the time step chosen. The resulting cloud droplet and aerosol particle spectra were stored every 100 s to yield the input for the radiation module. Thus, the grid spacing for the radiation module changes. It is equal to 50 m for the first 1000 m in the sub-cloud region next to the ground. In the cloud region which extends from 1000 m to 4100 m the grid distance changes so that the radiation code levels correspond to the altitudes where the droplet spectra were stored. Above the cloud region up to 59 km the grid distance increased.

In order to study the processing of the aerosol particle spectrum by the cloud, both, the cloud droplet spectrum and the moist interstitial aerosol particle spectrum at 4100 m where the ascending motion came to a halt were stored. For each size bin the residual aerosol particle mass after complete and instantaneous evaporation was calculated following:

$$m_{AP,res} = \frac{g_{APd}(m)}{f_d(m)},$$

for the drops, and

$$m_{AP,in} = \frac{g_{APa}(m_{AP})}{f_{APa}(m_{AP})},$$

for the interstitial aerosol particles. Assuming a spherical equivalent radius the combination of dried-off interstitial aerosol particles and cloud residues yields a new initial dry aerosol particle spectrum. Before introducing this aerosol particle spectrum into a new cloud cycle the particles larger than 4 μm are removed in order to correct for the processes of sedimentation disregarded so far in the parcel model dynamics.

2.4. *The microphysical and radiative module in the 2-D framework*

The slab-symmetric dynamic model employed in the present study is a two-dimensional version of the three-dimensional model developed by Clark and co-workers (Clark, 1977, 1979; Clark and Gall, 1982; Clark and Farley, 1984; Hall, 1980). The coupling of DESCAM with this dynamic framework is discussed in Flossmann and Pruppacher (1988). For the model results presented here, however, the gas phase concentrations were set to zero and only the interaction of drops and aerosol particles was studied. The model covered a domain of 10 km in the vertical and 20 km in the horizontal. The grid spacings were $\Delta z = 200$ m and $\Delta x = 400$ m resulting in 52×52 grid points. The overall time step was $\Delta t = 5$ s with a possible reduction in the condensation routine. The time step represents a compromise between rapid processes like cloud microphysics and turbulence and the computational effort to integrate such a large model over a 1-h time period. The 1-D radiation model was then applied to a cut through the model domain at $x = 12.8$ km. It uses the same grid spacing as the dynamic model up to 10 km. Above the grid spacing was the same as for the parcel model framework.

3. Initial conditions

3.1 *For the parcel model dynamics (0-D)*

The initial vertical profile for temperature and humidity for the medium sized cumulus cloud was the one used already by Lee et al. (1980). The initial dry aerosol particle spectrum for the reference case A was assumed to be of maritime type consisting of a superposition of three log-normal distributions as proposed by Jaenicke (1988).

$$\frac{\mathrm{d}N}{\mathrm{d}\ln r} = f_{\mathrm{APa}}(\ln r) = \sum_{i=1}^{3} \frac{n_i}{(2\pi)^{1/2} \log \sigma_i \ln 10} \times \exp\left(- \frac{[\log(r/R_i)]^2}{2(\log \sigma_i)^2} \right). \quad (1)$$

The parameters we used pertain to a typical marine air mass taken from Jaenicke(1988) and are summarised in Table 2. All particles were assumed to consist of 100% $(NH_4)_2SO_4$. The authors are aware of the fact that this assumption is not completely true for the marine aerosol population. As was already detailed by Fitzgerald (1991) the large marine particles are composed of sea salt while the small one consist of sulphate. We have, however, decided to simplify the scenario essentially for two reasons. First, the solute effect for aerosol particles in equilibrium with an atmosphere almost or at saturation is rather small. Second, our interest in the current study is the cycling of particles through more than one cloud

Table 2. *Parameters for the maritime aerosol particle distribution as given in eq. (1) for the air parcel dynamics*

Mode i	n_i	R_i	$\log \sigma_i$	Chemical compound	Case A	Case B
1	133	0.0039	0.657	$(NH_4)_2SO_4$	$1 \times n_1$	$2 \times n_1$
2	66.6	0.1330	0.210	$(NH_4)_2SO_4$	$1 \times n_2$	$1 \times n_2$
3	3.06	0.2900	0.396	$(NH_4)_2SO_4$	$1 \times n_3$	$1 \times n_3$

n_i = total number of aerosol particles per cm^3; R_i = geometric mean aerosol particle radius in μm; σ_i = standard deviation in mode i; chemical composition of the aerosol particle modes; the number concentrations as used in case A and B detailed in Table 4.

event. Considering different chemical compositions would create heterogeneous particles with a different degree of mixing complicating significantly the calculation for a second cloud event. Thus, we deliberately reduced the particles to consist only of sulphate. The concentration of gases were set to 0.5 ppb(v) for SO_2 and H_2O_2 and 30 ppb(v) for O_3. The model parcel was launched at 900 mb (=1000 m) with an initial relative humidity of 99% and a vertical velocity of 1 m/s. Several sensitivity tests were performed using modified parameters for eq. (1) (case B) or the processed particle spectrum after one cloud cycle (cases E, F, G, H). The details are summarised in Table 3.

The radiation model was initialised with the same temperature and humidity profiles as the air parcel model. Apart from the cloud droplet also an aerosol particle spectrum and trace gases (CO_2, NO_2, O_3) inside and outside the cloud region were considered. The aerosol particle spectra inside the cloud were the ones calculated from the microphysical model at the corresponding height. The vertical aerosol particle profiles outside cloud were taken from the initial conditions. The O_3 distribution was taken from Craig (1965) and a constant CO_2 concentration with height was used, as in Zdunkowski et al. (1982). The pollution gas NO_2 was taken as 0.2 parts per million at the surface and decreasing linearly within the first 1000 m, and zero concentration above. The surface temperature was set to 295.15 K. The surface emissivity was set to 0.98 (the mean emissivity value for water and ocean surfaces). The ground albedo over water was set to 0.1. The radiation code was initialised for 50° latitude and for the Julian date 212 (30 July) at 12.00 UTC.

3.2. *For the 2-D model dynamics*

The initialisation of the present model is the same as that in Flossmann (1998): The sounding was taken at day 261 (18 September 1974) of the GATE campaign at 12 GMT. Our 2-D model domain was oriented north-south, as this was the main wind direction. In the lowest 2 km and above 6 km the wind was southerly while in between the wind was northerly. The initial dry aerosol particle

Table 3. *Summary of the cases considered*

Case	Dynamics	Input aerosol particle spectrum
A	0-D	maritime
B	0-D	maritime, $2 \times n_1$
C	2-D	maritime
D	2-D	maritime, $2 \times n_1$, $2 \times n_2$
E	0-D	dried-off particle spectrum after 1900 s from case A
F	0-D	dried-off particle spectrum after 1900 s from case B
G	0-D	50% dried-off particle spectrum after 1900 s from case A and 50% initial particle spectrum from case A
H	0-D	50% dried-off particle spectrum after 1900 s from case B and 50% initial particle spectrum from case B

Table 4. *Parameters for the maritime aerosol particle distribution as given in eq. (1) for the 2-D dynamics*

Mode i	n_i	R_i	$log\ \sigma_i$	Chemical compound	H_i (400 m)	Case C (>400 m)	Case D (>400 m)
1	133	0.0039	0.657	$(NH_4)_2SO_4$	3000	$1 \times n_1$	$2 \times n_1$
2	66.6	0.1330	0.210	$(NH_4)_2SO_4$	3000	$1 \times n_2$	$2 \times n_2$
3	3.06	0.2900	0.396	NaCl	—	$0 \times n_3$	$0 \times n_3$

n_i = total number of aerosol particles per cm^3; R_i = geometric mean aerosol particle radius in μm; σ_i = standard deviation in mode i; chemical composition and scale height H_i (m) of the aerosol particle modes; the number concentrations above 400 m altitude for the cases C and D of Table 4.

Table 5. *Albedo and cloud optical thickness for 2 different times calculated with the radiation model for the cloud properties resulting after 200 s and 1900 s simulation time for case A and case B*

0-D	Case A/ 200 s	Case A/ 1900 s	Case B/ 200 s	Case B/ 1900 s
A	0.56	0.57	0.61	0.64
τ	11.05	17.06	14.37	24.61

spectrum was again given by eq. (1). The two small modes $i=1$ and 2 were assumed to consist of $(NH_4)_2SO_4$ particles and the large mode $i=3$ was set to hold only NaCl particles. The parameters are summarised in Table 4. This aerosol particle size distribution was assumed to exist homogeneously throughout the MBL (marine boundary layer), i.e., in the lower 400 m for the cases considered. For the height dependency above the MBL 2 different scenarios were studied. In the 1st case (case C), the $(NH_4)_2SO_4$ particles were assumed to decrease exponentially with height

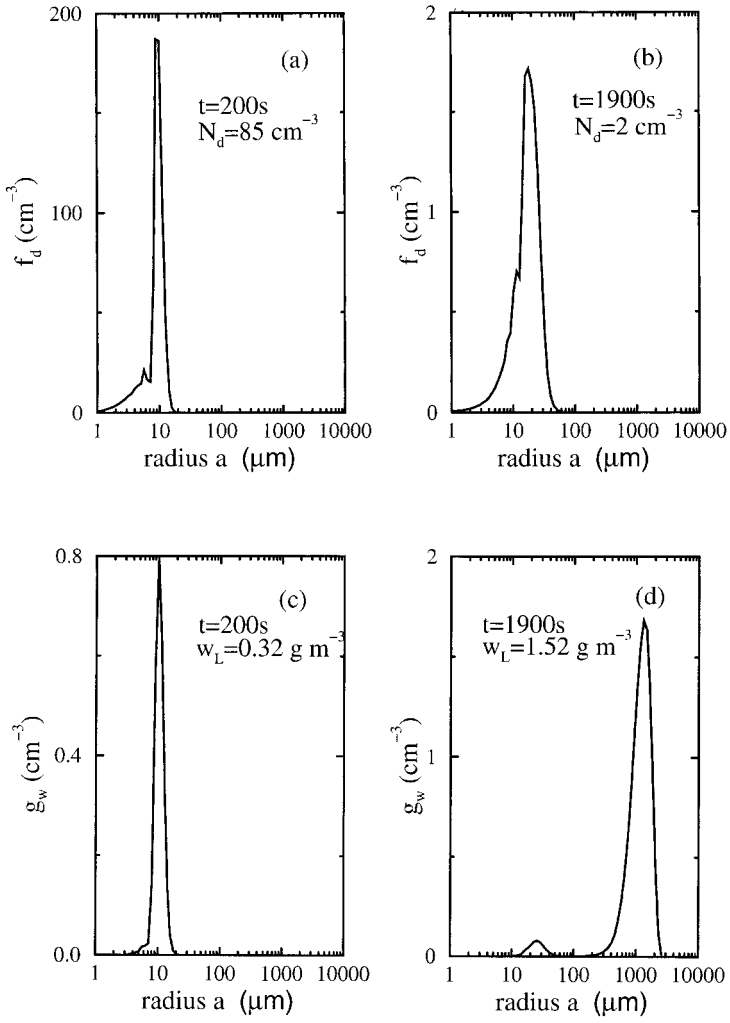

Fig. 1. Cloud drop number density distribution function $f_d(m)$ and cloud water mass density distribution function g_w for case A after 200 s and 1900 s of cloud life time.

with a scale height of 3 km while the NaCl particles were assumed to be zero above the boundary layer. In the *second case* (case D) the $(NH_4)_2SO_4$ particles above 400 m were doubled with respect to *case C* while the NaCl concentration was still assumed to zero. The parameters are summarised in Table 5.

The cloud was driven by a surface sensible and latent heat flux as a percentage of the incoming solar radiation. The method is described in Flossmann (1991). The radiation model was initialised in the same way as for the parcel model calculations. Only the date was adjusted, the latitude was set to 9°, and the surface temperature to 301 K.

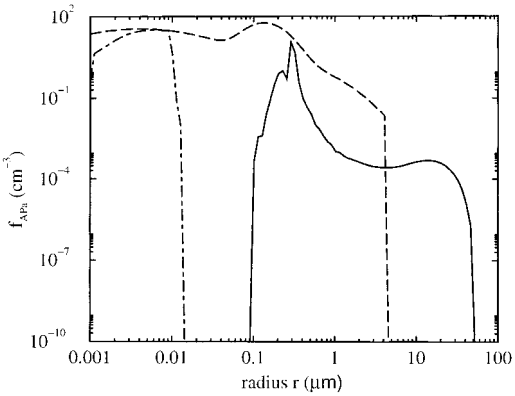

Fig. 2. Initial dry aerosol particle spectrum (dashed line), interstitial dry aerosol particle spectrum at 1900 s (dash dot line) and drop residual aerosol particle spectrum at 1900 s (solid line) as a function of the dry particle radius.

4. Model results

When the air parcel was launched for the reference case A at 1000 m it immediately reached saturation and then supersaturation. A cloud formed on about 85 condensation nuclei per cm^3 (Fig. 1a). During the ascent of the air parcel the processes of condensation, collision-coalescence, break-up, impaction scavenging, gas scavenging, oxidation and entrainment changed the droplet spectrum. When the parcel lost its buoyancy and came to a halt at around 4100 m after 1900 s of life time the drop spectrum had a liquid water content of 1.52 g/m^3 mainly comprised in the precipitation sized drops (Fig. 1b, d).

In order to study the maximum change imposed on the considered aerosol particle spectrum by the cloud cycle we have instantaneously dried the cloud hydrometeors and re-established a modified aerosol particle distribution. This size distribution is a composite of the evaporated cloud residues and the never-activated interstitial aerosol particles.

Fig 2 shows the initial aerosol size distribution and the distribution modified by the cloud event. We find several modifications in different size ranges. The very small particles have decreased due to impaction scavenging by cloud drops (due to brownian motion which is especially important for small aerosol particles). In the size range between 0.01 and 0.1 μm radius we find an important gap in the distribution. It is caused by the fact that all aerosol particles larger than 0.012 μm have been activated to form drops. The low activation size is due to the evolution of the supersaturation. Directly above cloud base the supersaturation achieved 0.6% dropping rapidly to values well below 0.3%. Only below cloud top the supersaturation increased again dramatically to values above 1% caused by the collision-coalescence effect reducing significantly the drop surface for vapour deposition. Thus, after 1900 s all particles larger 0.012 μm have activated to drops and have grown to particles of 0.1 μm and above. This growth is caused by in cloud processes such as collision/coalescence, impaction scavenging and gas uptake. We found for our present study with low gas concentrations in a remote marine environment, however, that the contribution of SO_2 uptake and oxidation to the in-cloud particle growth was negligible. This is in agreement with our earlier studies (Flossmann et al., 1987). Consequently, the effects of gas uptake will be neglected in the remaining discussion.

The sharp lower and upper limits of the gap are model-induced. The lower limit at 0.01 μm results from the fact that only one volume of homogeneous particles is considered neglecting heterogeneous mixing effects (Baker et al., 1980). The upper limit at 0.1 μm results from the fact that inside one drop class only the total aerosol particle mass is followed loosing the information

Table 6. *Albedo and cloud optical thickness for case C and case D calculated with the 2-D dynamic framework after 45 min of simulation time (19 min of cloud life time)*

2-D	Case C	Case D
A	0.52	0.56
τ	11.72	14.0

Table 7. *Albedo and cloud optical thickness for 2 different times calculated with the radiation model for the cloud properties resulting after 200 s and 1900 s simulation time for case E and case F*

0-D	Case E/ 200 s	Case E/ 1900 s	Case F/ 200 s	Case F/ 1900 s
A	0.35	0.5	0.44	0.60
τ	4.08	9.93	6.37	17.28

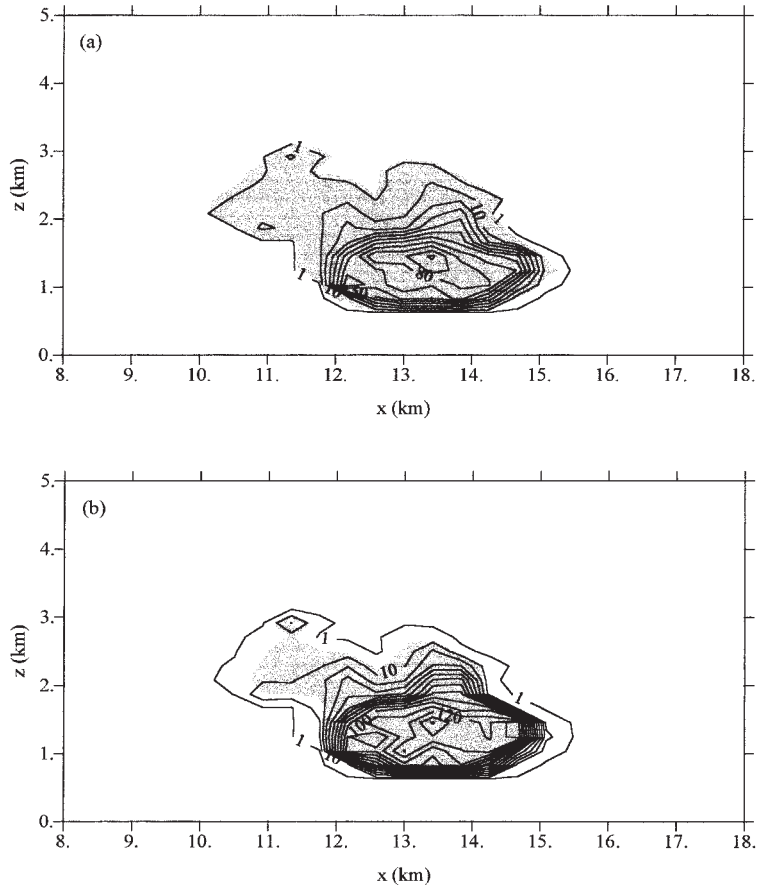

Fig. 3. Drop number concentration in #/cm^3 after 45 min of model time (19 min of cloud life time) for case C (a) and case D (b) considered; contour spacing 10 #/cm^3; the outmost contour line is 1 #/cm^3; the shaded area is the visible cloud ($q_c > 0.1$ g/kg).

about the original size. Thus, drying a drop class results in a monodisperse aerosol.

Even though the sharp edges of the gap are induced by the model architecture we are convinced that the existence, position and approximate size of the gap is realistic. Numerous measurements of cloud modified marine particle spectra have confirmed this so-called ≪Hoppel minimum≫ (Hoppel et al., 1990; Hoppel and Frick, 1990).

Concerning the cloud processed aerosol particle spectrum we can see that a redistribution of the aerosol particle mass took place. The number of small particles has decreased and the number of large particles consequently increased due to an effective collision-coalescence process going on between the drops. This process also is reflected in the cloud drop spectrum at 1900 s (Fig. 1b, d). The dried-off aerosol particles of as large as 40 μm in Fig. 2 are, however, an artefact of the parcel model which does not allow to consider the effect of sedimentation.

The resulting cloud radiative properties for this case A are summarised in Table 5.

In an attempt to study the effect of an increasing number of small aerosol particles on the development of the precipitating cloud and its radiative properties, we have doubled the number of particles in the first mode (case B). As could be expected (Charlson et al., 1987) the number of small droplets formed almost doubled (159 cm^{-3} instead of 85 cm^{-3} at 200 s). Thus, an albedo results which is 5% larger than the one of the reference case (Table 5). Also, the optical thickness increased significantly. Consequently, we confirm that an increase in the initial number of aerosol particles smaller than 1 μm results in an increase in cloud albedo. The time and amount of precipitation formed, however, did not change significantly.

In order to verify that this result is not an artefact of the parcel model geometry, we did a similar study in the 2-D model framework (case C). The model simulation started at 12 GMT. After 26 min of model time a cloud had formed. After 14 min of cloud life time the first rain fell from cloud base and after 19min of cloud life time the first rain reached the ground. Fig. 3a displays the cloud drop number distribution for the case C after 19 min of cloud life time. Fig. 3b gives the distribution for an enhanced number of small particles (case D). We see confirmed that the number of droplets formed has significantly increased. Fig. 4 shows the rain rate for the two cases C and D. We see that the evolution of the rainfall is still quite similar. This can be attributed to the fact that for both cases the initial aerosol particle distribution stays in the range of typical marine concentrations which easily form precipitation (compare Flossmann (1998)).

The resulting radiative properties for case C and D can be found in Table 6. Here, we observe an increase of cloud albedo and optical thickness in the same order of magnitude as the parcel model calculation (compare Table 5), the dimension of the cloud in the 2-D framework being similar (∼3000 m) to the one calculated with the parcel model. Thus, we can conclude that despite its simplifying geometry the parcel model is adequate for the type of problem to be studied. Thus, for the following sensitivity studies again the parcel model framework will be used.

In order to study the possible effect of clouds on the processing of aerosol particles we have re-introduced the dried-off aerosol particle distribution after the cloud event simulated with the air parcel model in case A and B into a new cloud cycle (case E and F). Fig. 5 gives f_d and g_w for the 2nd cloud cycle for cases E and F. In general, we see that the number of drops in the second cloud

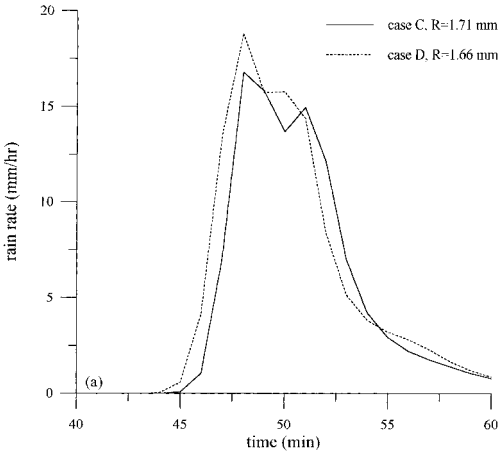

Fig. 4. Time evolution of the rain rate in mm/hr, for the cases C and D considered; *R* is the total precipitation (mm).

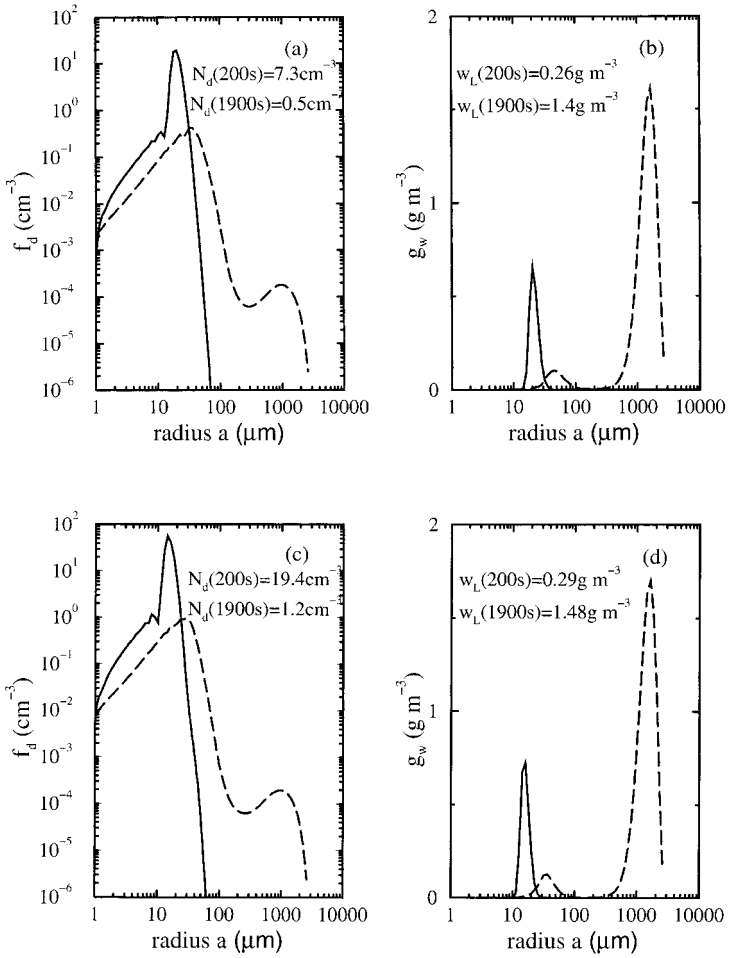

Fig. 5. Cloud drop number density distribution function $f_d(m)$ and cloud water mass density distribution function g_w for case E (a and b) and F (c and d) after 200 s (solid line) and 1900 s (dashed line) of cloud life time.

cycle is significantly reduced with respect to the first. This is mainly due to the precipitation in the first cloud. It accumulated a large number of particles in the large drops. The resulting "tail" in the evaporated particle spectrum (Fig. 2) was truncated at 4 μm before entering a second cloud cycle. Still, we note that the number of drops formed in case F remains slightly higher than for the case E, reflecting the initial conditions of case A and B. In general, the production of precipitation sized drops is slightly enhanced in the second cloud cycle due to the reduced number of drops.

Table 8. *Albedo and cloud optical thickness for 2 different times calculated with the radiation model for the cloud properties resulting after 200 s and 1900 s simulation time for case G and case H*

0-D	Case G/ 200 s	Case G/ 1900 s	Case H/ 200 s	Case H/ 1900 s
A	0.52	0.58	0.57	0.62
τ	8.62	15.15	11.1	20.21

Table 7 gives the resulting radiative properties of the clouds. The low cloud albedo and optical thickness indicate the extremes possible in such precipitating clouds. We can conclude that clouds process the aerosol particle population in a way

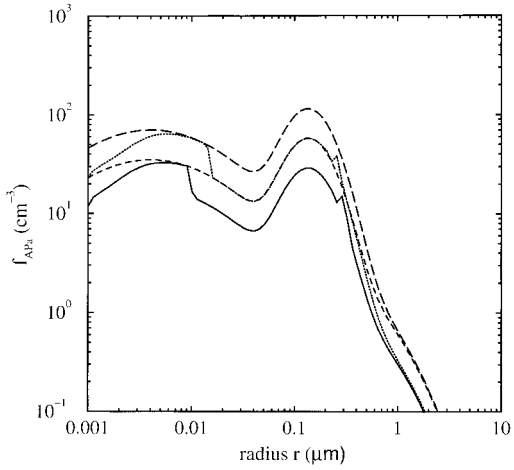

Fig. 6. Initial dry aerosol particle spectrum for case A (short dashes), case B (long dashes), case G (solid line) and case H (dotted line) as a function of the dry particle radius.

which reduces the total number of particles. This counteracts an increase of small particle, e.g.. by new particle production. Naturally, introducing the processed aerosol particle spectrum directly into a renewed cloud cycle greatly exaggerates the effect as normally the processed aerosol particles mix with the ambient undisturbed aerosol before serving again as CCN. We tried to take into account this effect by taking a mixture of 50% processed aerosol particles and 50% undisturbed aerosol particles as input for a second cloud cycle (case G and H). The cloud, then, resembles more the one for the first cloud cycle (case A and B; compare Table 5) with respect to the number of drops formed. Also the radiative properties given in Table 8 approach those for case A and B staying, however, below.

It is interesting to note that the cloud radiative properties of the second cloud cycle of the enhanced number case H resembles those of the first cloud cycle of the undisturbed case A indicating the tendency of clouds to counteract, e.g., an anthopogenically induced increase of particle number. This resemblance becomes understandable looking at Fig. 6. Here, we see the input spectra for case A, B, G, and H. Case H approaches in large parts the reference spectrum A. This is caused by the choice of parameters for case B and the mixture imposed for case G and H. For different parameters this result will change, however, we believe that the tendency will persist.

5. Summary and conclusions

We have simulated with our DESCAM model coupled to a dynamic framework the evolution of different clouds. The resulting drop spectra then entered a radiation code to yield the up- and downwelling radiative fluxes, the cloud optical depth and the cloud albedo. If we start from the scenario that in a marine environment the number of small aerosol particles increases, this can increase the albedo of a cloud forming in this air mass of about 5% with respect to the albedo of clouds forming in an unperturbed aerosol population. This capacity to increase the cloud albedo, however, is not persistent. The cloud itself changes the particle spectrum. The smallest aerosol particles are reduced by impaction scavenging. The particles between 0.01 μm and 0.1 μm are depleted due to the fact that they serve as CCN and grow through in-cloud processes. Here, our studies have shown, however, that growth due to absorption and oxidation of gases (e.g., SO_2) plays a minor role. We have found that already in Flossmann et al. (1987) and it has been confirmed for this study (Hatzianastassiou, 1997). This is in agreement with studies of Feingold et al. (1996) who found that collision and coalescence of drops is the dominant growth mechanism in a region with low gas concentrations like the remote oceans.

Thus, cloud processes change the aerosol particle spectrum in such a way that in a second cloud cycle the albedo is lower. In the case studied here, however, the mechanism of precipitation formation was not much altered as already the initial particle spectrum produced rain easily.

Consequently, from these preliminary studies we can conclude that indeed an enhanced number of small aerosol particles increases cloud albedo as predicted by Charlson et al. (1987). However, the clouds themselves work towards a reduction in particle number, thus, reducing the perturbation. However, more studies are necessary to quantify the processes and to determine the conditions under which they occur. Also, we have to keep in mind that the study presented here applies

to a shallow precipitating cumulus cloud. Further studies for non-precipitating and stratus clouds need to be made in the future.

6. Acknowledgements

The authors acknowledge with gratitude the support by the European Community under ENV4-CT95–0117 and ENV4-CT95–0012. They are solely responsible for the content of this manuscript. The calculations for this paper have been done on the CRAY C98 and C94 of the "Institut du Développement et des Ressources en Informatique Scientifique" (IDRIS, CNRS) in Orsay (France) under project no. 940180. The authors acknowledge with gratitude the hours of computer time and the support provided. Furthermore, the authors acknowledge the support provided by the French national program PATOM.

REFERENCES

Ackerman, A. S., O. B. Toon and P. V. Hobbs, 1995. Numerical modeling of ship tracks produced by injections of cloud condensation nuclei into marine stratiform clouds. *J. Geophys. Res.* **100**, 7121–7133.

Baker, M.B., R.G. Corbin and J. Latham, 1980. The influence of entrainment of the evolution of cloud droplet spectra (I). A model of inhomogeneous mixing. *Quart. J. R. Meteor. Soc.* **106**, 581–598.

Charlson, R. J., J. E. Lovelock, M. O. Andrae and S. G. Warren, 1987. Oceanic phytoplankton, atmosheric sulphur, cloud albedo and climate. *Nature* **326**, 655–661.

Clark, T. L. 1977. A small scale dynamic model using terrain-following coordinate transformation. *J. Comput. Phys.* **24**, 186–215.

Clark, T. L. 1979. Numerical simulations with a three dimensional cloud model. *J. Atmos. Sci.* **36**, 2191–2215.

Clark T. L. and Gall, R. 1982. Three dimensional numerical model simulations of air flow over mountainous terrain: A comparison with observation. *Mon. Weather Rev.* **110**, 766–791.

Clark, T. L and Farley, R. D. 1984. Severe downslope windstorm calculations in two and three spatial dimensions using anelastic interactive grid nesting. *J. Atmos. Sci.* **41**, 329–350.

Craig, R. A. 1965. The upper atmosphere, meteorology and physics. Academic Press, New York and London.

Feingold, G., S. M. Kreidenweiss, B. Stevens and W. R. Cotton, 1996. Numerical simulations of stratocumulus processing of cloud condensation nuclei through collision-coalescence. *J. Geophys. Res.* **101**, 21391–21402.

Fitzgerald, J. W. 1991. Marine aerosols. A review. *Atmos. Environ.* **25A**, 533–545.

Flossmann, A. I. 1991. The scavenging of two different types of marine aerosol particles using a two-dimensional detailed cloud model. *Tellus* **43B**, 301–321.

Flossmann, A. I. 1994. A 2-D spectral model simulation of the scavenging of gaseous and particulate sulfate by a warm marine cloud. *J. Atmos. Res.* **32**, 255–268.

Flossmann, A. I. 1998. Interaction of aerosol particles and clouds. *J. Atmos. Sci.* **55**, 879–887.

Flossmann, A.I. and H.R. Pruppacher, 1988. A theoretical study of the wet removal of atmospheric pollutants. Part III. *J. Atmos. Sci.* **45**, 1857–1871.

Flossmann, A. I., W. D. Hall and H. R. Pruppacher, 1985. A theoretical study of the wet removal of atmospheric pollutants. Part I. *J. Atmos. Sci.* **42**, 582–606.

Flossmann, A. I., H. R. Pruppacher and J. H. Topalian, 1987. A theoretical study of the wet removal of atmospheric pollutants. Part II. *J. Atmos. Sci.* **44**, 2912–2923.

Hall, W. D. 1980. A detailed microphysical model within a two-dimensional dynamic framework. Model description and preliminary results. *J. Atmos. Res.* **37**, 2486–2507.

Hatzianastassiou, N. 1997. *Etude de l'effet indirect des particules d'aérosol sur le bilan radiatif lors de cycles nuageux consécutifs*. PhD thesis, No. D.U. 935, LaMP (Clermont-Ferrand).

Hatzianastassiou, N., W. Wobrock and A. I. Flossmann, 1997. The role of droplet spectra for cloud radiative properties. *Q.J.R. Meteorol. Soc.* **123**, 2215–2230.

Hoppel, W. A. and G. M. Frick, 1990. Submicron aerosol size distributions measured over the tropical and south Pacific. *Atmos. Environm.* **24A**, 645–659.

Hoppel, W. A., J. W. Fitzgerald, G. M. Frick, R. E. Larson and E. J. Mack, 1990. Aerosol size distributions and optical properties found in the marine boundary layer over the Atlantic Ocean. *J. Geophys. Res.* **95**, 3659–3677.

IPCC, 1995. *Climate change 1995. The science of climate change*, eds.: J. T, Houghton, L. G. Meira Filho, B. A. Callander, N. Harris, A. Kattenberg and K. Maskell, Cambridge University Press.

Jaenicke, R. 1988. Aerosol physics and chemistry. In: Landolt-Boernstein: *Zahlenwerte und Funktionen aus Naturwissenschaften und Technick*, **V 4b**, G. Fischer, ed. Springer, Berlin, pp. 391–457.

Lee, I. Y., G. Hanel and H. R. Pruppacher, 1980. A numerical determination of the evolution of cloud drop spectra due to condensation on natural aerosol particles. *J. Atmos. Sci* **37**, 1839–1853.

Zdunkowski W. G. and P. Breslin, 1979. A numerical test of two approximate solutions to the radiative transfer equation using the Elsasser scheme. *Pure Appl. Geophys.* **117**, 927–934.

Zdunkowski, W. G., R. M. Welch and G. Korb, 1980. An investigation of the structure of typical two-stream methods dor the calculation of solar fluxes and heating rates in clouds. *Beitr. Phys. Atmos.* **53**, 147–166.

Zdunkowski W. G., W. G. Panhans, R. M. Welch and G. J. Korb, 1982. A radiation scheme for circulation and climate models. *Beitr. Phys. Atmos.* **55**, 215–238.